Hindawi Publishing Corporation
Journal of Sensors
Volume 2015, Article ID 874637, 6 pages
http://dx.doi.org/10.1155/2015/874637

Research Article

Image Quality Assessment of a CMOS/Gd_2O_2S:Pr,Ce,F X-Ray Sensor

Christos Michail

Radiation Physics, Materials Technology and Biomedical Imaging Laboratory, Department of Biomedical Engineering, Technological Educational Institute of Athens, Egaleo, 122 10 Athens, Greece

Correspondence should be addressed to Christos Michail; michail@upatras.gr

Received 25 March 2015; Revised 27 June 2015; Accepted 6 July 2015

Academic Editor: Mike McShane

The aim of the present study was to examine the image quality performance of a CMOS digital imaging optical sensor coupled to custom made gadolinium oxysulfide powder scintillators, doped with praseodymium, cerium, and fluorine (Gd_2O_2S:Pr,Ce,F). The screens, with coating thicknesses 35.7 and 71.2 mg/cm^2, were prepared in our laboratory from Gd_2O_2S:Pr,Ce,F powder (Phosphor Technology, Ltd.) by sedimentation on silica substrates and were placed in direct contact with the optical sensor. Image quality was determined through single index (information capacity, IC) and spatial frequency dependent parameters, by assessing the Modulation Transfer Function (MTF) and the Normalized Noise Power Spectrum (NNPS). The MTF was measured using the slanted-edge method. The CMOS sensor/Gd_2O_2S:Pr,Ce,F screens combinations were irradiated under the RQA-5 (IEC 62220-1) beam quality. The detector response function was linear for the exposure range under investigation. Under the general radiography conditions, both Gd_2O_2S:Pr,Ce,F screen/CMOS combinations exhibited moderate imaging properties, in terms of IC, with previously published scintillators, such as CsI:Tl, Gd_2O_2S:Tb, and Gd_2O_2S:Eu.

1. Introduction

Indirect medical imaging detectors incorporate a scintillator detector coupled to an optical sensor (CCD, CMOS, etc.). The scintillator is used in the form of either screens or needle phosphor layers [1]. Optical ceramic scintillators have been also developed in order to replace single crystals in some applications [1–4]. Ceramic gadolinium oxysulfide doped with praseodymium, cerium, and fluorine (Gd_2O_2S:Pr,Ce,F) (ultrafast ceramics, UFC) has been proposed for Computed Tomography (CT) applications [4]. Gd_2O_2S:Pr,Ce,F is an efficient and fast scintillator (decay time of the order of 3-4 μs) based on the well-known traditional Gd_2O_2S host material [5].

A semiconductor technology that has been used widely recently is complementary metal oxide (CMOS) semiconductors [6–9]. The initial CMOS pixel structure was in the form of passive pixel sensors (PPSs) and was followed by the active pixel sensors (APS), which have been developed with the goal of improving the image quality [10]. APS CMOS sensors provide high resolution even at high framing rates and, in association with scintillating screens, have been increasingly investigated for medical imaging applications [11]. In the present study, image quality of a CMOS digital imaging sensor, coupled to Gd_2O_2S:Pr,Ce,F powder phosphor screens, was investigated by single index and spatial frequency dependent parameters.

The single index information capacity (IC) was considered as an overall image quality metric, including the effects of sharpness, contrast, and noise of the CMOS sensor coupled to Gd_2O_2S:Pr,Ce,F powder phosphor screens. IC was estimated by the experimental measurement of the Signal Transfer Property (STP), the Modulation Transfer Function (MTF), and the Normalized Noise Power Spectrum (NNPS).

2. Materials and Methods

2.1. Phosphor Screens. Gd_2O_2S:Pr,Ce,F was purchased in powder form (Phosphor Technology Ltd., England, code: UKL59CF/N-R1) with a mean grain size (estimated by ultrasonic dispersion with a coulter counter having 100 μm aperture) of approximately 9.7 μm (Phosphor Technology

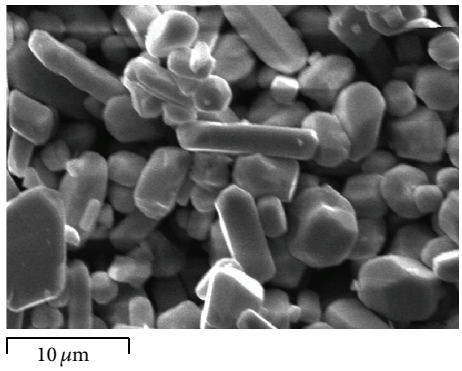

Figure 1: Scanning electron microscope image of the Gd_2O_2S:Pr,Ce,F phosphor.

Ltd., datasheet) [5]. Gd_2O_2S:Pr,Ce,F has effective atomic number $Z_{eff} = 61.1$, density of 7.34 g/cm^3, and a decay time of the order of a 3×10^{-6} s [3].

The phosphor was used in the form of thin layers to simulate the intensifying screens employed in X-ray imaging. Two screens with coating thicknesses 35.7 and 71.2 mg/cm^2 were prepared by sedimentation of Gd_2O_2S:Pr,Ce,F powder on fused silica substrates (spectrosil B). Sodium orthosilicate (Na_2SiO_3) was used as binding material between the powder grains.

Gd_2O_2S:Pr,Ce,F powder phosphor particles morphology was verified via scanning electron microscope (SEM) micrographs using the Jeol JSM 5310 SEM combined with the INCA software (Figure 1).

2.2. CMOS Sensor. The Gd_2O_2S:Pr,Ce,F scintillating screens were manually coupled to an optical readout device including a CMOS Remote RadEye HR photodiode pixel array [9, 12]. The CMOS photodiode array consists of 1200 × 1600 pixels with 22.5 μm pixel spacing. The Gd_2O_2S:Pr,Ce,F screens were directly overlaid onto the active area of the CMOS photodiode array, consisting of an N-well diffusion on p-type epitaxial silicon, and held by using a thin polyurethane foam layer for compression between the screen and a 1 mm thick graphite cover. A 70 kV (RQA-5) X-ray beam was used, following the IEC standards [13]. IEC standard X-ray spectrum was achieved by adding 21 mm Al filtration in the beam to simulate beam quality alternation by a human body. A BMI General Medical Merate tube with rotating tungsten anode and inherent filtration equivalent to 2 mm Al was used for the RQA-5 beam quality. The source-to-detector distance (SDD) between the X-ray focal spot and the surface of the detector was set to 176 cm. The added filtration was placed as close as possible to the source.

2.3. Image Quality

2.3.1. Signal Transfer Property (STP). The Signal Transfer Property (STP) provides the relationship between mean pixel value (MPV) and Entrance Surface Air Kerma (ESAK) at the detector surface. This relationship was obtained by plotting pixel values (PV) versus ESAK at the detector, as described in the IEC method [13]. A sequence of uniform images was acquired at different exposure levels. MPV was evaluated in a 1 × 1 cm region of interest (ROI). The system's response curve was fitted using a linear equation of the following form:

$$\mathrm{MPV} = \alpha + b \times K_\alpha, \tag{1}$$

where α and b are fit parameters and K_α is the incident air kerma (ESAK). From the slope of the system's response curve, the value of the gain factor (G) was obtained. This value is relating MPV to the incident exposure at the detector (in digital units per μGy) [14]. The magnitude of the pixel offset at zero air kerma was also estimated [15].

2.3.2. Modulation Transfer Function (MTF). The spatial frequency transfer characteristics of linear and spatially invariant imaging systems can be characterized by the system's Modulation Transfer Function (MTF) [16, 17]. MTF describes the variation of contrast with spatial frequency and hence expresses spatial resolution. MTF of an imaging system is defined as the absolute value of its optical transfer function, normalized to unity at spatial frequency zero [14]:

$$\mathrm{MTF}(v) = \frac{M(x)}{M(0)}. \tag{2}$$

In this study, the MTF was measured using the slanted-edge technique, following the procedures described in IEC standard [13, 15]. A PTW Freiburg tungsten edge test device was used to obtain the slanted-edge images. The edge test device consists of a 1 mm thick W edge plate (100 × 75 mm^2) fixed on a 3 mm thick lead plate. Images of the edge, placed at a slight angle in order to avoid aliasing effects, were obtained. The edge spread function (ESF) was calculated by the extraction of a 1 × 1 cm^2 ROI with the edge roughly at the center. The restricted ROI area could not accurately measure the low frequency drop, in powder screens; however, the size is limited from the size of the screen which is 2 × 2 cm^2 and the active area of the CMOS sensor (2.7 × 3.6 cm). Neglecting the low frequency drop could result in overestimation of the MTF and thus also of the DQE values.

2.3.3. Normalized Noise Power Spectrum (NNPS). The NPS was calculated according to IEC 62220-1-1:2015 [13]. For each ROI, the pixel values were converted into air-kerma units. The slowly varying spatial background effects including the heel effect were corrected by fitting and subtracting a two-dimensional second-order polynomial to the original acquired image data [18]. All images were acquired with offset and gain correction. The area of analysis was 1024 × 1024 pixels. Half-overlapping ROIs with a size of 128 × 128 pixels were then taken from the subimages [13]. A total of 128 ROIs were taken from each flood image. For all the ROIs taken from each image 2D fast Fourier transform (FFT) of each ROI was calculated and added to the NPS ensemble. NNPS was obtained by dividing NPS by the square of the corresponding K_α and afterwards the ensemble average was obtained.

2.3.4. Detective Quantum Efficiency (DQE) and Image Quality Figure of Merit (IQFOM). The Detective Quantum Efficiency has been defined as the efficiency of a system to transfer the Signal-to-Noise Ratio (SNR) through the imaging chain [19]. The DQE of the system can be calculated by the following equation:

$$\mathrm{DQE}(u) = \frac{\mathrm{MTF}^2(u)}{K_\alpha \times q \times \mathrm{NNPS}(u)}, \quad (3)$$

where q is the number of photons per unit kerma (μGy) per mm^2 [9]. A value of 29563 photons $\times$ μGy^{-1} $\times$ mm^{-2} is required, for the RQA-5 beam quality, according to [13]. However, in the present study, a value of 21627 photons $\times$ μGy^{-1} $\times$ mm^{-2} was calculated from direct X-ray spectra measurements with a portable Amptek XR-100T spectrometer and the extracted ESAK values were validated against direct measurements with a Victoreen 4000M+ dosimeter [12]. Accordingly, (3) was used for calculations; however, an alternative term was employed, namely, Image Quality Figure of Merit (IQFOM), due to the difference in the q values proposed by the IEC protocol [13].

2.3.5. Information Capacity (IC). The concept of image information capacity (IC) has been introduced within the context of Shannon's information theory, in order to assess image information content [20]. In digital imaging, the continuous spatial distribution of an optically generated image is sampled by the discrete sensitive pixels on a photodiode array, whose outputs are converted into digitized signals and stored in an image processing system for numerical evaluation. According to Shannon's information theory, the image information capacity, per unit of image area, may be defined as follows [20]:

$$\mathrm{IC} = \lim_{T\to\infty} \frac{\log_2 N_s}{T} = n_p \log_2 N_s, \quad (4)$$

where N_s are the different signal intensity levels, T is the duration of the signal, and n_p is the number of pixels of the imaging system. In this study, information capacity was calculated according to [21]

$$\mathrm{IC} = \frac{1}{2}\int_0^u \log_2\left(1 + \frac{\mathrm{SPS}(u)}{\mathrm{NPS}(u)}\right) 2\pi u\, du, \quad (5)$$

where SPS is the signal power spectrum which can be defined as SPS = $(\mathrm{MTF} \times G)^2$, where G is the gain factor [22].

3. Results and Discussion

Figure 2 shows the detector response curves (STP) of the CMOS sensor combined with the 35.7 and 71.2 mg/cm^2 Gd_2O_2S:Pr,Ce,F screens, respectively, under the RQA-5 (70 kVp) beam quality. The detector was found to have a linear response, covering the whole exposure range, with a pixel value offset of −8.193 and 15.19 for the 35.7 and 71.2 mg/cm^2 Gd_2O_2S:Pr,Ce,F screens, respectively.

The linear no-threshold fits gave correlation coefficients (R^2) greater than 0.9992 and 0.9994 for the 35.7 and 71.2 mg/cm^2 Gd_2O_2S:Pr,Ce,F screens. The gain factor G was determined as the slope of the characteristic curve, relating the mean pixel value to the incident exposure. Using flat-field images, the gain factors were determined by linear regression to be G = 4.710 and 7.902 digital units per μGy for the 35.7 and 71.2 mg/cm^2 Gd_2O_2S:Pr,Ce,F screens under the RQA-5 beam quality. However, the values of G are restricted by the bit depth of the CMOS sensor under investigation, compared to large flat panel detectors, dedicated for medical imaging [23].

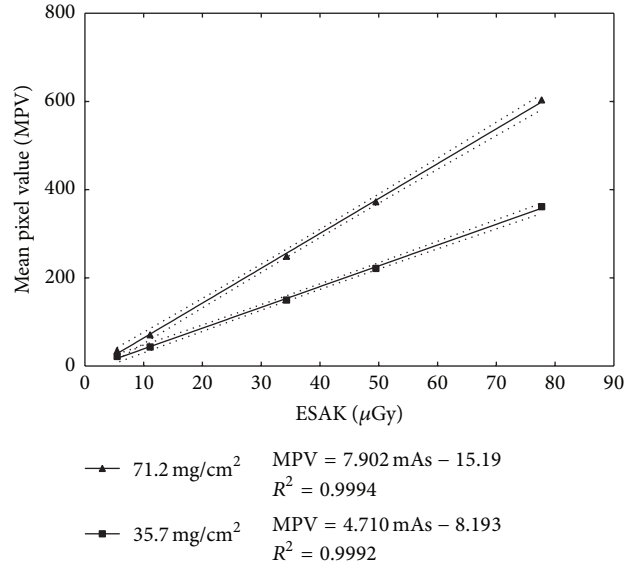

Figure 2: Detector response curves (STP) of the CMOS sensor combined with the 35.7 and 71.2 mg/cm^2 Gd_2O_2S:Pr,Ce,F screens, respectively, under the RQA-5 (70 kVp) beam quality.

Figure 3 shows MTF curves, for the 35.7 and 71.2 mg/cm^2 Gd_2O_2S:Pr,Ce,F screens, coupled to the CMOS sensor. Under the RQA-5 conditions, the 35.7 mg/cm^2 screen/CMOS combinations show higher MTF values, compared to the thicker 71.2 mg/cm^2 Gd_2O_2S:Pr,Ce,F screen, across the spatial frequency range, except for some frequencies, where the thick screen shows systematic discrepancies in the MTF values, which may be due to screen nonuniformities. For comparison purposes, data for Gd_2O_2S:Tb [12] and CsI:Tl [24] scintillators detectors are shown. Both Gd_2O_2S:Tb and CsI:Tl screens were produced industrially (not custom made). Furthermore CsI:Tl is in columnar form; thus, light can be easily transmitted to the output in order to produce narrow light pulses, which in turn lead to improved resolution. The Gd_2O_2S:Pr,Ce,F screen combinations showed lower MTF values compared to previously published scintillators. However, both Gd_2O_2S:Pr,Ce,F screens show comparable MTF results with the 65.1 mg/cm^2 Europium doped Gd_2O_2S (Gd_2O_2S:Eu) screen [21] in all the spatial frequency range, showing that the resolution properties of this material could be considered for general radiography applications.

Figure 4 shows the extracted 1D Normalized Noise Power Spectrum (NNPS), for the u direction, obtained from uniformly exposed images, at an exposure level of 11.1 μGy,

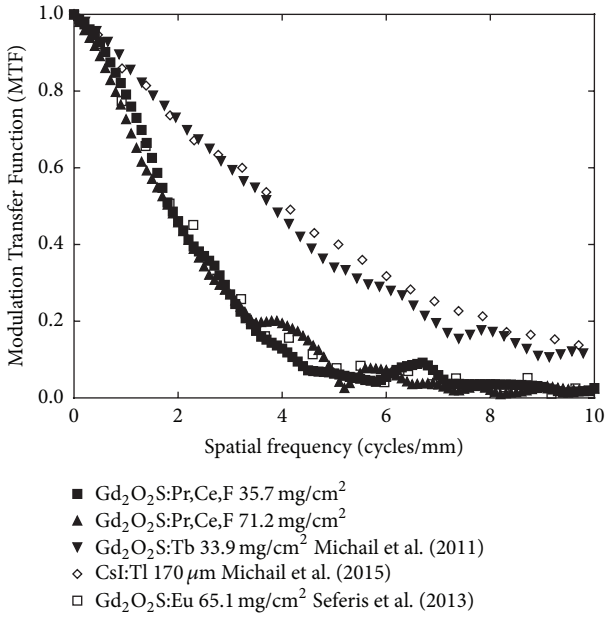

Figure 3: MTF curves, of the 35.7 and 71.2 mg/cm^2 Gd_2O_2S:Pr,Ce,F screen coupled to the CMOS sensor, compared with previously published detectors.

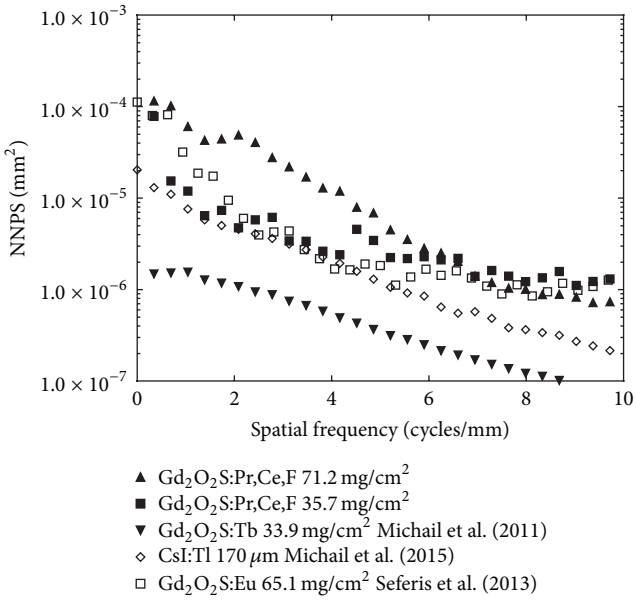

Figure 4: NNPS curves of the 35.7 and 71.2 mg/cm^2 Gd_2O_2S:Pr,Ce,F screens coupled to the CMOS sensor, compared with previously published detectors.

which is close to the usual clinical dose ranges for medical imaging systems [23]. The NNPS curves are falling with increasing spatial frequency. A slight decrease from 4.56×10^{-6} mm^2 (at 2.08 cycles/mm^2) to 1.1×10^{-6} (at 9 cycles/mm^2) was observed in the NNPS values of the 35.7 mg/cm^2 Gd_2O_2S:Pr,Ce,F screen coupled to the CMOS sensor. This is attributed to the combined noise effects of

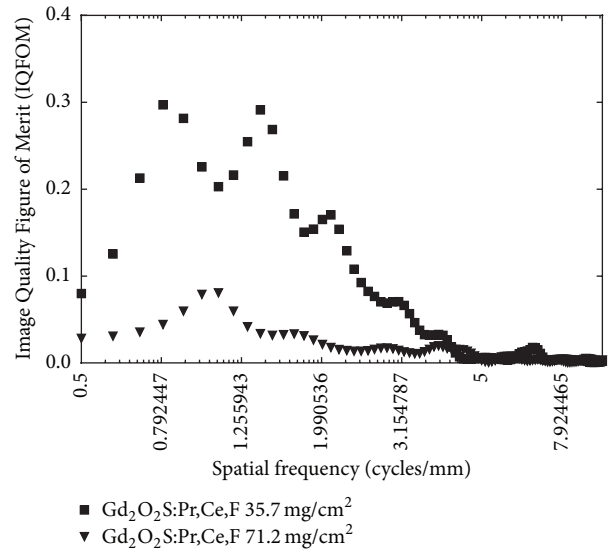

Figure 5: IQFOM curves of the 35.7 and 71.2 mg/cm^2 Gd_2O_2S:Pr,Ce,F screens coupled to the CMOS sensor.

the screen and the CMOS sensor, in which a 2D correction is applied reducing the structured noise in each image. Noise levels in the 35.7 mg/cm^2 Gd_2O_2S:Pr,Ce,F screen are in acceptable levels and can be compared with the CsI:Tl screen, for spatial frequencies up to 4 cycles/mm. In the thicker 71.2 mg/cm^2 Gd_2O_2S:Pr,Ce,F screen coupled to the CMOS sensor, NNPS levels are rather higher due to the presence of low frequency components (spatial frequencies up to 4.5 cycles/mm) that can be attributed to screen inhomogeneities, due to the sedimentation production process. A decrease from 4.92×10^{-5} mm^2 (at 2.08 cycles/mm^2) to 8.26×10^{-7} (at 9 cycles/mm^2) was observed in the NNPS values of the 71.2 mg/cm^2 Gd_2O_2S:Pr,Ce,F screen coupled to the CMOS sensor. Noise levels of the 65.1 mg/cm^2 Gd_2O_2S:Eu screen are in between both Gd_2O_2S:Pr,Ce,F screens, being in accordance with the noise properties following screen thickness. As was expected, Gd_2O_2S:Tb screen shows the lowest noise levels, combining screen thickness, internal properties of the material, and the industrial production process.

Figure 5 shows IQFOM curves obtained for the 35.7 and 71.2 mg/cm^2 Gd_2O_2S:Pr,Ce,F screens, coupled to the CMOS sensor. DQE and IQFOM values are principally affected by the variation of the ratio of the squared MTF over NNPS. IQFOM of the 35.7 mg/cm^2 screen/CMOS combination was found to maximize in the medium spatial frequency range and drop thereafter, whereas the corresponding IQFOM values of 71.2 mg/cm^2 screen/CMOS combination maximize in the low spatial frequency range.

Table 1 shows information capacity values for the combination of the CMOS sensor with the 35.7 and 71.2 mg/cm^2 Gd_2O_2S:Pr,Ce,F screens under investigation and previously published IC values for a CMOS sensor coupled to Gd_2O_2S powder scintillators, activated either with terbium (Tb) or Europium (Eu). The comparison, under the RQA-5 beam quality, was obtained at the same exposure level for all

Table 1: Information capacity values.

Beam quality	Coating weight (mg/cm^2)	Information capacity (bits/mm^2) CMOS-scintillator combinations		
		Gd_2O_2S:Tb	Gd_2O_2S:Eu	Gd_2O_2S:Pr,Ce,F
RQA-5	33.91	2806 ± 34	—	—
	65.1	—	1826 ± 18	—
	35.7	—	—	1813 ± 23
	71.2	—	—	1722 ± 35

screen/sensor combinations. The thinner Gd_2O_2S:Tb screen (33.91 mg/cm^2) showed the highest IC values due to the screen thickness and the higher MTF values of this screen, compared to the 35.7 mg/cm^2 Gd_2O_2S:Pr,Ce,F. The IC values of the thicker 71.2 mg/cm^2 Gd_2O_2S:Pr,Ce,F were lower than all the other screens, even from the IC value of the 65.1 mg/cm^2 Gd_2O_2S:Eu screen due to the fact of the higher thickness and screen uniformity, leading to lower MTF values and higher noise. These data show that, for a given level of incident X-ray fluence, information capacity is mainly determined by the intrinsic phosphor material properties and by the screen thickness of the imaging system. In thick screens, the lateral light trajectories are very long causing a large fraction of the laterally directed photons to be absorbed before reaching the screen output.

4. Conclusion

In the present study, image quality of two custom made Gd_2O_2S:Pr,Ce,F powder scintillator screens, coupled to a CMOS digital imaging sensor, was investigated under X-ray radiography imaging conditions. Image quality was investigated in terms of single index and spatial frequency dependent parameters. The detector response function was linear for the exposure range under investigation. The overall imaging properties, in terms of the single index IC, of both Gd_2O_2S:Pr,Ce,F screen/CMOS combinations were found moderate compared to previously published scintillators, such as Gd_2O_2S:Tb, CsI:Tl, and Gd_2O_2S:Eu.

Conflict of Interests

The author declares that there is no conflict of interests regarding the publication of this paper.

Acknowledgments

This research has been cofunded by the European Union (European Social Fund) and Greek National Resources under the framework of the "ARISTEIA" project MISCIRLU Code 1476 of the "Education and Lifelong Learning" Operational Programme.

References

[1] M. Nikl, "Scintillation detectors for x-rays," *Measurement Science and Technology*, vol. 17, no. 4, pp. R37–R54, 2006.

[2] H. Yamada, A. Suzuki, Y. Uccida, M. Yoschida, and H. Yammoto, "A scintillator Gd_2O_2S:Pr,Ce,F for X-ray computed tomography," *Journal of the Electrochemical Society*, vol. 136, pp. 2713–2720, 1989.

[3] C. Greskovich and S. Duclos, "Ceramic scintillators," *Annual Review of Materials Science*, vol. 27, no. 1, pp. 69–88, 1997.

[4] I. Veronese, *Radiation Physics for Nuclear Medicine*, Springer, Heidelberg, Germany, 2011.

[5] C. Michail, I. Valais, I. Seferis et al., "Measurement of the luminescence properties of Gd_2O_2S:Pr,Ce,F powder scintillators under X-ray radiation," *Radiation Measurements*, vol. 70, pp. 59–64, 2014.

[6] S. E. Bohndiek, E. J. Cook, C. D. Arvanitis et al., "A CMOS active pixel sensor system for laboratory-based X-ray diffraction studies of biological tissue," *Physics in Medicine and Biology*, vol. 53, no. 3, pp. 655–672, 2008.

[7] I. A. Elbakri, B. J. McIntosh, and D. W. Rickey, "Physical characterization and performance comparison of active- and passive-pixel CMOS detectors for mammography," *Physics in Medicine and Biology*, vol. 54, no. 6, pp. 1743–1755, 2009.

[8] B. K. Cha, J. Y. Kim, T. J. Kim, C. Sim, and G. Cho, "Fabrication and imaging characterization of high sensitive CsI(Tl) and Gd_2O_2S(Tb) scintillator screens for X-ray imaging detectors," *Radiation Measurements*, vol. 45, no. 3–6, pp. 742–745, 2010.

[9] I. Seferis, C. Michail, I. Valais et al., "Light emission efficiency and imaging performance of Lu_2O_3:Eu nanophosphor under X-ray radiography conditions: comparison with Gd_2O_2S:Eu," *Journal of Luminescence*, vol. 151, pp. 229–234, 2014.

[10] M. Zhang and A. Bermak, "CMOS image sensor with on-chip image compression: a review and performance analysis," *Journal of Sensors*, vol. 2010, Article ID 920693, 17 pages, 2010.

[11] M. Endrizzi, P. Oliva, B. Golosio, and P. Delogu, "CMOS APS detector characterization for quantitative X-ray imaging," *Nuclear Instruments and Methods in Physics Research A: Accelerators, Spectrometers, Detectors and Associated Equipment*, vol. 703, pp. 26–32, 2013.

[12] C. M. Michail, V. A. Spyropoulou, G. P. Fountos et al., "Experimental and theoretical evaluation of a high resolution CMOS based detector under X-ray imaging conditions," *IEEE Transactions on Nuclear Science*, vol. 58, no. 1, pp. 314–322, 2011.

[13] IEC, *Medical Electrical Equipment—Characteristics of Digital X-Ray Imaging Devices—Part 1-1: Determination of the Detective Quantum Efficiency—Detectors Used in Radiographic Imaging*, IEC 62220-1-1 Ed.1.0, 2015.

[14] U. Neitzel, S. Günther-Kohfahl, G. Borasi, and E. Samei, "Determination of the detective quantum efficiency of a digital x-ray detector: comparison of three evaluations using a common image data set," *Medical Physics*, vol. 31, no. 8, pp. 2205–2211, 2004.

[15] E. Samei, M. J. Flynn, and D. A. Reimann, "A method for measuring the presampled MTF of digital radiographic systems using an edge test device," *Medical Physics*, vol. 25, no. 1, pp. 102–113, 1998.

[16] W. Hendee, *Medical Imaging Physics*, Wiley-Liss, 4th edition, 2002.

[17] I. A. Cunningham and B. K. Reid, "Signal and noise in modulation transfer function determinations using the slit, wire, and edge techniques," *Medical Physics*, vol. 19, no. 4, pp. 1037–1044, 1992.

[18] N. W. Marshall, "A comparison between objective and subjective image quality measurements for a full field digital mammography system," *Physics in Medicine and Biology*, vol. 51, no. 10, pp. 2441–2463, 2006.

[19] J. T. Dobbins III, *Handbook of Medical Imaging*, SPIE, Bellingham, Wash, USA, 2000.

[20] C. E. Shannon, "A mathematical theory of communication," *Bell System Technical Journal*, vol. 27, pp. 379–423, 1948.

[21] I. E. Seferis, C. M. Michail, I. G. Valais et al., "On the response of a europium doped phosphor-coated CMOS digital imaging detector," *Nuclear Instruments and Methods in Physics Research, Section A: Accelerators, Spectrometers, Detectors and Associated Equipment*, vol. 729, pp. 307–315, 2013.

[22] R. F. Wagner, D. G. Brown, and M. S. Pastel, "Application of information theory to the assessment of computed tomography," *Medical Physics*, vol. 6, no. 2, pp. 83–94, 1979.

[23] A. C. Konstantinidis, M. B. Szafraniec, R. D. Speller, and A. Olivo, "The Dexela 2923 CMOS X-ray detector: a flat panel detector based on CMOS active pixel sensors for medical imaging applications," *Nuclear Instruments and Methods in Physics Research Section A: Accelerators, Spectrometers, Detectors and Associated Equipment*, vol. 689, pp. 12–21, 2012.

[24] C. Michail, I. Valais, I. Seferis, N. Kalyvas, G. Fountos, and I. Kandarakis, "Experimental measurement of a high resolution CMOS detector coupled to CsI scintillators under X-ray radiation," *Radiation Measurements*, vol. 74, pp. 39–46, 2015.